IJMMM International Journal of Minerals, Metallurgy and Materials 矿物冶金与材料学报（英文版）

Simulation on scrap melting behavior and carbon diffusion under natural convection

Ming Gao, Jin-tao Gao, Yan-ling Zhang, and Shu-feng Yang

Cite this article as:
Ming Gao, Jin-tao Gao, Yan-ling Zhang, and Shu-feng Yang, Simulation on scrap melting behavior and carbon diffusion under natural convection, *Int. J. Miner. Metall. Mater.*, 28(2021), No. 3, pp. 380-389. https://doi.org/10.1007/s12613-020-1997-0

International Journal of Minerals, Metallurgy and Materials
Volume 28, Number 3, March 2021, Page 380
https://doi.org/10.1007/s12613-020-1997-0

Simulation on scrap melting behavior and carbon diffusion under natural convection

Ming Gao[1)], *Jin-tao Gao*[1)], *Yan-ling Zhang*[1)], *and Shu-feng Yang*[2)]

1) State Key Laboratory of Advanced Metallurgy, University of Science and Technology Beijing, Beijing 100083, China
2) School of Metallurgical and Ecological Engineering, University of Science and Technology Beijing, Beijing 100083, China
(Received: 21 November 2019; revised: 31 January 2020; accepted: 2 February 2020)

Abstract: A 3D model applying temperature- and carbon concentration- dependent material properties was developed to describe the scrap melting behavior and carbon diffusion under natural convection. Simulated results agreed reasonably well with experimental ones. Scrap melting was subdivided into four stages: formation of a solidified layer, rapid melting of the solidified layer, carburization, and carburization + normal melting. The carburization stage could not be ignored at low temperature because the carburization time for the sample investigated was 214 s at 1573 K compared to 12 s at 1723 K. The thickness of the boundary layer with significant concentration difference at 1573 K increased from 130 μm at 5 s to 140 μm at 60 s. The maximum velocity caused by natural convection decreased from 0.029 $m \cdot s^{-1}$ at 5 s to 0.009 $m \cdot s^{-1}$ at 634 s because the differences in temperature and density between the molten metal and scrap decreased with time.

Keywords: scrap melting; natural convection; carbon diffusion; numerical simulation; electron probe micro-analyzer

1. Introduction

In China, the amount of scrap has rapidly increased with the development of the iron and steel industry. Scrap recycling should be promoted, especially scrap melting in steelmaking. The scrap melting behavior under natural convection is the basis for understanding its melting mechanism in practice [1–3].

Many numerical models involving heat and mass transfer have been used to analyze the effect of various factors (scrap size, preheating temperature, and bath temperature) on scrap melting under natural convection [4–8]. Studies on the scrap melting behavior and complex phase change problem under natural convection indicated that scrap melting could be divided into three stages: formation of a solidified layer, rapid melting of the solidified layer, and normal melting. Mori and Nomura [4] reported that the types and sizes of scrap affect scrap melting and the transient heat conduction in the solid scrap. Wu and Lacroix [8] established a 2D time-dependent heat transfer model in a circular furnace and showed that the melting is significantly accelerated at high heat transfer coefficients. In addition, scrap melting is facilitated by carbon diffusion from the hot metal to the scrap surface [9–13]. Kruskopf and other researchers [10–12] established a 2D melting model involving a chemical reaction and reported that the scrap melting rate is affected by the heat transfer and carbon diffusion. Deng *et al*. [13] analyzed the scrap melting mechanism using a solidification/melting model and a Shear-stress transport (SST) k–ω model in the ANSYS FLUENT software. However, detailed information on the scrap melting process under natural convection is greatly limited. Few studies have directly observed the carburization using numerical methods, although it tends to be the basis of scrap melting. Sun *et al*. [14] analyzed the carbon distribution in the radial direction and the melting process of a small sphere in hot metal. Penz *et al*. [15] investigated the scrap melting at the solid–liquid interface. They both reported an obvious interface between the parent scrap and the frozen shell. The carbon content in the frozen shell is much higher than that in the parent scrap. In addition, the material properties, e.g., density, specific heat, diffusion coefficient, and thermal conductivity, are defined as constants in most studies. However, this condition greatly differs from actual ones. These material properties should be defined as functions of temperature and composition.

This study performed a numerical simulation of scrap melting, along with laboratory-scale experiments. A 3D model coupling the heat and mass transfer was established to

Corresponding author: Yan-ling Zhang E-mail: zhangyanling@metall.ustb.edu.cn

describe the scrap melting behavior under natural convection and observe the carburization, wherein temperature- and carbon concentration-dependent material properties were considered. Furthermore, the scrap melting mechanism, melting time, and natural convection formation were discussed.

2. Experimental and simulation model description

2.1. Laboratory-scale experiments

As shown in Fig. 1(a), a vertical tube furnace (BCMT-1973 K, China) was used for experiments. Approximately 1 kg of pig iron used for steelmaking (C: 4.61wt%) was melted in an alumina crucible (inner diameter: 65 mm; outer diameter: 70 mm; and height: 100 mm) to ensure that the bath depth reached 50 mm. Steel cylinders 100 mm in length and 10 mm in diameter were prepared from Q235 low-carbon steel (C: 0.168wt%). The scrap cylinder was immersed into 30 mm and held for different durations. The range of bath temperatures was 1573–1723 K, as measured by a thermocouple inside the furnace. The experimental method is shown in Fig. 1(b). The material composition and experimental operation were described in Ref. [16].

2.2. Simulation model description

2.2.1. Geometry model and operating condition

As shown in Fig. 2, the model simulated is the part below the hot metal. Similar to the experiments, the geometry model was 65 mm in diameter and 50 mm in height. The steel cylinder was 10 mm in diameter and immersed in the hot metal at a depth of 30 mm. The bath temperatures ranged from 1573 to 1723 K.

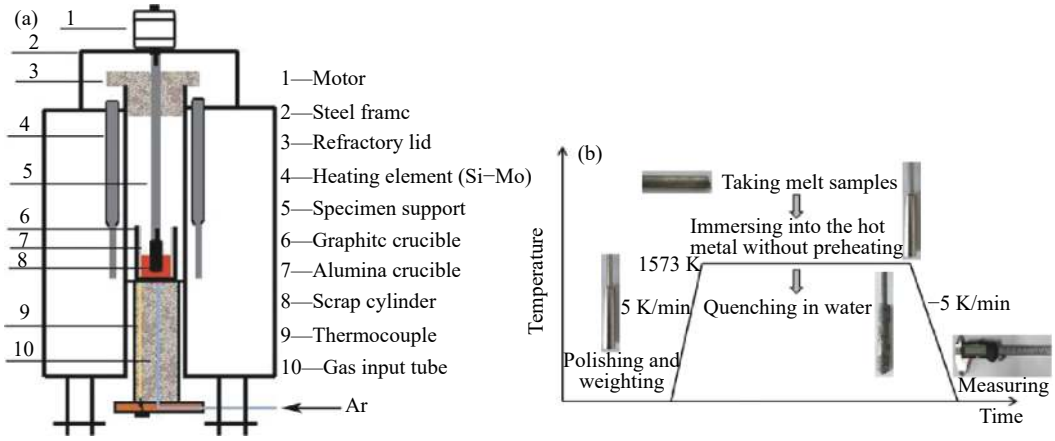

Fig. 1. Schematic of scrap melting experimental apparatus (a) and experimental method (b).

The ANSYS FLUENT16.0 software has been successfully used to simulate mass transfer and flow [17]. In the present work, the mesh number of 191540 was selected. The setting of calculation parameters is shown in Table 1. The *X*–*Y* plane (*Z* = 0) was selected as the surface to observe the melting behavior. In addition, the liquid phase was assumed to be Newtonian fluid. No heat loss on the walls or heat exchange between the melted surface and air above the molten pool was assumed. Therefore, the boundary conditions of the crucible wall and hot metal surface were considered to be a wall with a fixed temperature.

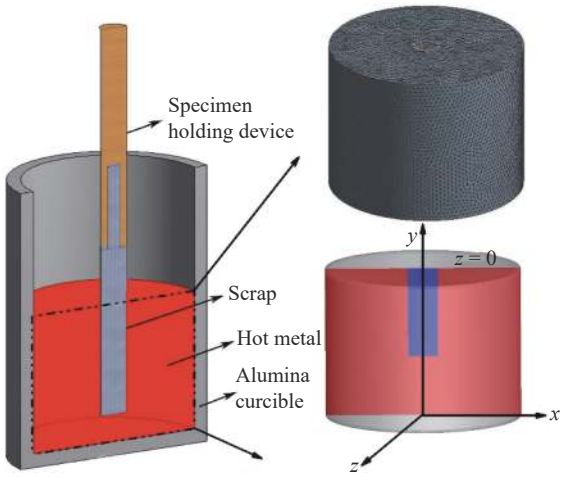

Fig. 2. Schematic of geometrical model about scrap melting process.

Table 1. Setting of calculation parameters for scrap melting model

Calculation parameter	Method
Solver	Pressure-based solver; Transient;
Pressure-velocity coupling schemes	SIMPLE
Gradient	Least squares cell bused
Spatial discretization schemes for pressure	PRESTO!
Momentum, energy, and species	Second-order upwind
Transient formulation	First-order implicit

As shown in Table 2, the material properties were calculated by JMatPro7.0 (Sente Software Ltd.). The data were fitted to functions by using the least square method. Density, specific heat, thermal conductivity, viscosity, and diffusion coefficient were defined as functions of temperature and carbon content.

Table 2. Material properties used in the scrap melting model

Calculation parameter	Value
Density / ($kg \cdot m^{-3}$)	7891.11–0.3628T–4538.291ω_c, $\omega_c \leq 1$wt%; 8060.8681–0.559T–2830.051ω_c, $\omega_c > 1$wt%.
Specific heat capacity / ($J \cdot kg^{-1} \cdot K^{-1}$)	260+0.55T, 300 K$\leq T <$900 K; –2172.7+3.26T, 900 K$\leq T <$1040 K; 4735–3.428T, 1040 K$\leq T <$1184 K; 327+0.231T, $T \geq$1184.
Thermal conductivity / ($W \cdot m^{-1} \cdot K^{-1}$)	13.84+0.012T–51.94ω_c, $\omega_c <$0.5wt%, $T >$1193 K; 66.24–0.032T–1194.2ω_c, $\omega_c <$0.5wt%, $T \leq$1193 K; 13.8278+0.01168T–46.1389ω_c, 0.5$\leq \omega_c \leq$1wt%, $T >$1083 K; 58.27–0.0224T–997.786ω_c, 0.5$\leq \omega_c \leq$1wt%, $T \leq$1083 K; 1.5546+0.0211T–97.9443ω_c, 1$< \omega_c \leq$3.675wt%, $T >$1038 K; 34.583+0.00225T–506.5673ω_c, 1$< \omega_c \leq$3.675wt%, $T \leq$1038 K; –13.3537+0.0313T–69.9609ω_c, $\omega_c >$3.675wt%, $T >$1054 K; 18.23347+0.0119T–250.385ω_c, $\omega_c >$3.675wt%, $T \leq$1054 K.
Viscosity / ($kg \cdot m^{-1} \cdot s^{-1}$)	0, $\omega_c \leq$1wt%, $T <$1573 K; 0.0113–2.926×10^{-6}T–0.03131ω_c, 1$< \omega_c \leq$1.753wt%, $T \geq$1513 K; 0, 1$< \omega_c \leq$3.675wt%, $T <$1513 K; 0.01706–6.2738×10^{-6}T–0.05421ω_c, $\omega_c \geq$1.753wt%, $T \geq$1421 K; 0, $\omega_c \geq$1.753wt%, $T <$1421 K.
Diffusion coefficient / ($m^2 \cdot s^{-1}$)	0, $\omega_c \leq$1wt%; 0, $\omega_c \geq$1.753wt%,$T <$1421 K; 0, 1$< \omega_c \leq$1.753wt%,$T <$1513 K; 10^{-4}×exp(–(12100/T+2.568)+(1320/T–0.554)×ω_c), $\omega_c \geq$1.753wt%, $T \geq$1421 K[18]; 3.5×10^{-9}, 1$< \omega_c \leq$1.753wt%, $T \geq$1513 K[4].

2.2.2. Basic equations

The solidification/melting model and species transfer model were used in the simulation. The enthalpy porosity method was used to solve continuous equations, energy equations, momentum equations, and component equations. Detailed introduction of the mathematical formulation can be found in ANSYS FLUENT Theory Guide [19]. Meanwhile, the liquid–solid mushy zone was treated as a porous zone with porosity equal to the liquid fraction (β). As shown in Eq. (1), the mushy zone is a region in which the liquid fraction lies between zero and one. The liquid and solid zones are the regions in which the liquid fraction is zero and one, respectively [17].

$$\beta = \begin{cases} 0, & T < T_{\text{solidus}}; \\ \dfrac{T - T_{\text{solidus}}}{T_{\text{liquidus}} - T_{\text{solidus}}}, & T_{\text{solidus}} < T < T_{\text{liquidus}}; \\ 1, & T > T_{\text{liquidus}}. \end{cases} \tag{1}$$

where T_{solidus} and T_{liquidus} are the solidus and liquidus temperatures in K, respectively. The energy and liquid fraction equations were solved iteratively to determine the temperature.

For the multi-component mixture, a mushy zone exists between the solidus and the liquidus. If the temperature is higher than T_{liquidus}, the domain totally consists of melt. The solidus and liquidus of the mixture can be expressed by Eq. (2) [19]:

$$T_{\text{solidus}} = T_{\text{melt}} + \sum\nolimits_{\text{solutes}} m_i Y_i / K_i;\ \boldsymbol{T}_{\text{liquidus}} = T_{\text{melt}} + \sum\nolimits_{\text{solutes}} m_i Y_i \tag{2}$$

where T_{melt} is the melting point of scrap in K, Y_i represents the mass fraction of solute i, K_i represents the partition coefficient of solute i, and m_i is the slope of the liquidus surface with respect to Y_i. It can be calculated by the eutectic temperature (T_{eutectic}) and the eutectic mass fraction ($Y_{i,\text{eutectic}}$) as shown in Eq. (3) [19].

$$m_i = \frac{T_{\text{eutectic}} - T_{\text{melt}}}{Y_{i,\text{eutectic}}} \tag{3}$$

For the species transfer involving melting, ANSYS FLUENT16.0 offers two models for species segregation at the micro-scale, namely, the Lever rule and the Scheil rule. They assume infinite diffusion and zero diffusion of the solute species in the solid, respectively. Here the Lever rule is applied and the species transport equation is shown in Eq. (4).

$$\frac{\partial}{\partial t}(\rho Y_i) + \nabla \cdot \left(\rho \beta \underset{v_{\text{liq}}}{\rightarrow} Y_{i,\text{liq}} \right) = -\nabla \cdot \left\{ -\rho [\beta D_{i,\text{m,liq}} \cdot \nabla \cdot Y_{i,\text{liq}} + (1-\beta) D_{i,\text{m,sol}} \cdot \nabla \cdot K_i Y_{i,\text{sol}}] \right\} \tag{4}$$

where $D_{i,\text{m,liq}}$ and $D_{i,\text{m,sol}}$ are the diffusion coefficients of i in liquid and solid in $m^2 \cdot s^{-1}$, respectively; v_{liq} is the velocity of liquid in $m \cdot s^{-1}$; $Y_{i,\text{liq}}$ and $Y_{i,\text{sol}}$ are the mass fractions of solute i in liquid and solid, respectively; and ρ is the density in $kg \cdot m^{-3}$; t

is the time in s.

3. Results and discussion

3.1. Model validation

The results obtained from the experiments and simulation are shown in Fig. 3. The cross-sectional area was obtained by the product of the average diameter and length according to the measured results. The ratios of the cross-sectional area at different durations and its initial value (S/S_0) were compared. The simulated results agreed well with the experimental ones. A solidified layer was formed and led to a dimensionless ratio (S/S_0) greater than one. The remelting of the solidified layer caused the S/S_0 to be less than one until the melting ended. Moreover, the results obtained from simulation showed that the scrap melting was promoted at high temperatures and that the carburization could not be ignored at low temperatures. The S/S_0 tendency and the above results were consistent with those obtained experimentally.

The scrap cylinder immersed in the high-carbon molten pool was under the condition of carburization. The stage in which the melting rate was so small that changes in the scrap cylinder shape were negligible was defined as "carburization." A "hump" was found in the simulation and experiments because of carburization, and it was more obvious at low temperatures. However, the hump was more obvious in the simulation than in the experiment, especially at low temperatures, because of the following reasons. First, the bath temperature decreased when the scrap cylinders were immersed. The molten pool was continuously heated using a vertical tube furnace to maintain the set temperature for the experiments. Thus, the bath temperature in the experiments was higher than that in the simulation model for the same scrap cylinder immersed in the hot metal. The carburization that was promoted in the experiments decreased the hump. Second, a mushy zone formed between the solid and liquid phases during scrap melting. In the simulation model, the scrap was defined as mushy when the liquid fraction was 0–1. It was still considered solid phase in the contour of the liquid fraction. The solid scrap melted and was considered liquid only when the liquid fraction was one [19]. However, the mushy parts of the scrap cylinder were so soft that they could not be considered solid phase in the practical experiments. Therefore, the hump in the experiments was lower than that in the simulation.

Furthermore, the results were similar to those reported by Chen [20]. He indicated that the pig iron solidifies on the scrap surface and melts rapidly. Then, the carbon diffuses from the hot metal to the scrap surface, which is under the condition of carburization. The solid scrap melts quickly once the bath temperature reaches the melting point of scrap [20].

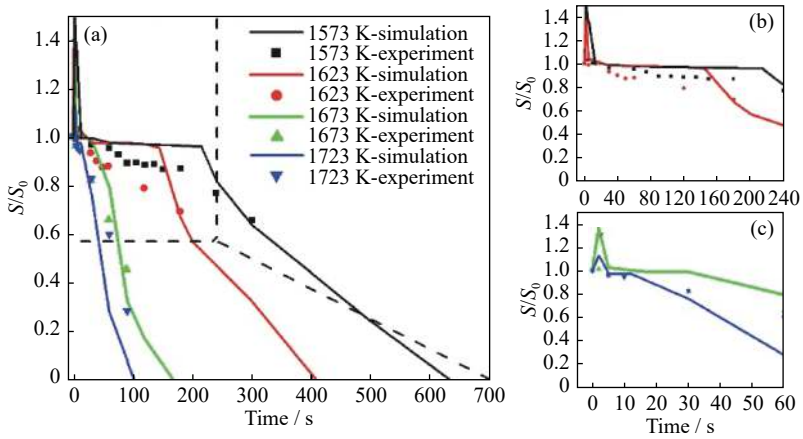

Fig. 3. Changes in the dimensionless ratio (S/S_0) at different bath temperatures: (a) total results at different temperature; (b) partial enlarged view at 1573 and 1623 K; (c) partial enlarged view at 1673 and 1723 K.

3.2. Scrap melting process and mechanism

Figs. 4 and 5 describe the melting of the scrap cylinder with 1573 K as an example. As shown in Fig. 4, the hot metal froze on the surface of the scrap cylinder and melted completely within 12 s until the parent scrap was exposed. However, the scrap cylinder did not melt immediately. The liquid fraction of the solid phase gradually increased within 214 s. The solid phase melted quickly when the bath temperature reached the melting point of the scrap. Then, the scrap cylinder melted along with the carburization until the melting ended (634 s). Therefore, the scrap melting was divided into four stages: formation of a solidified layer, rapid melting of the solidified layer, carburization, and carburization + normal melting. The phenomenon was also found in the experimental results. As shown in Fig. 5, the solidified layer formed and remelted within about 10 s. Then, the scrap cylinder melted slowly until 180 s. The scrap cylinders then melted rapidly along with the carburization. The four stages of scrap melting are also shown in Fig. 3. Consistent with previous

studies, the process was composed of three stages: formation of a solidified layer, rapid melting of the solidified layer, and normal melting [10–12]. The carburization was included in the third stage of normal melting. However, the carburization in this study was placed in a single stage and could not be ignored at low temperatures.

The formation and remelting of the solidified layer can be explained by the heat balance in the thermal boundary layer [5,8–9,12,21–24]. The heat flux density on the inside and outside of the phase interface should be equal [1]. A partial melt must release the latent heat to compensate for the loss of heat flux density on the outside due to the immersion of the scrap. Thus, a solidified layer formed at the surface of the scrap cylinder and was heated by the heat from the interior of the scrap cylinder. It melted when the heat flux density due to heat conduction was less than that generated by the convective heat transfer.

The shape of the scrap cylinder in a stationary melt is a frustum of a cone because the buoyancy effects induced by the temperature and concentration gradients promotes the flow of liquid in the stationary molten pool. The phenomenon is defined as natural convection [25]. In Figs. 6 and 7, the formation of natural convection can be explained by the changes in density and velocity. Taking 1573 K as an example, the molten pool was stationary and the density was uniform at 0 s. As shown in Fig. 6, the density in the molten pool was not uniform at 5 s, indicating the formation of a density difference. Then, a high-density liquid flowed along the vertical solid–liquid interface. In Fig. 7, the corresponding region produced a flow from the top to the bottom. The maximum velocity caused by natural convection reached 0.029 $m \cdot s^{-1}$. The natural convection gradually weakened with

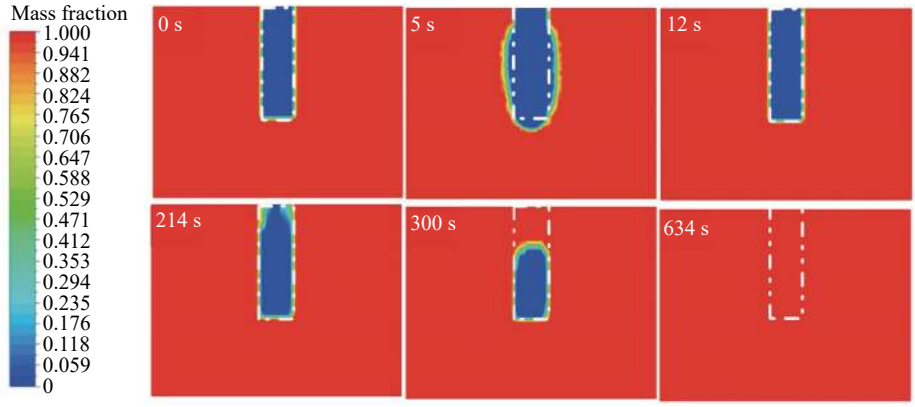

Fig. 4. Changes in the contour of liquid fraction with immersed time (1573 K).

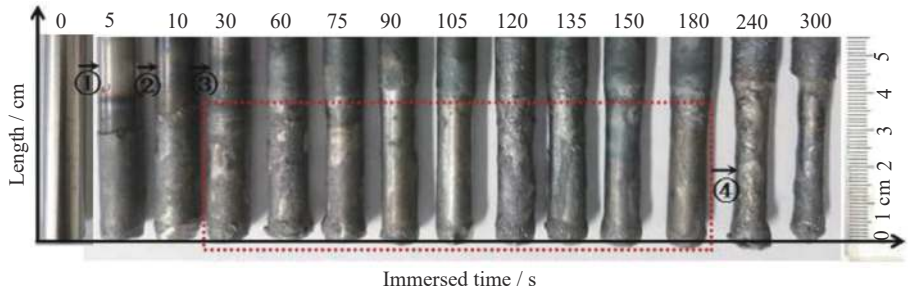

Fig. 5. Changes in the shape of the scrap cylinder with immersed time (1573 K).

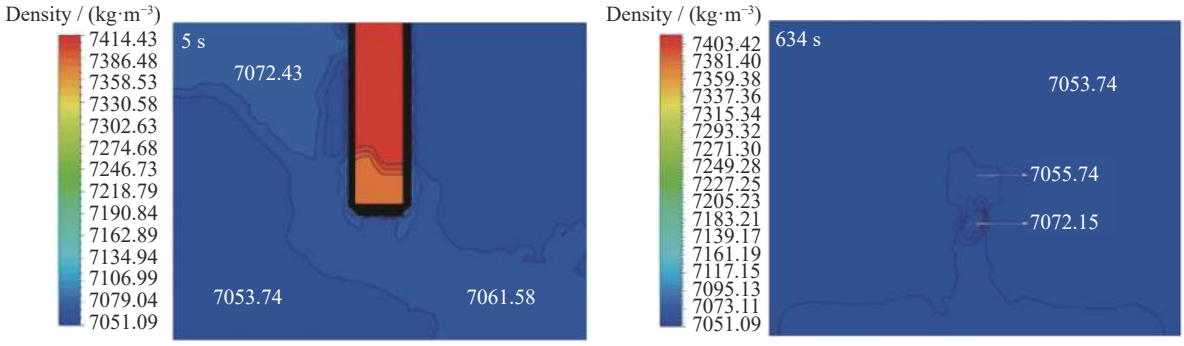

Fig. 6. Changes in the density of liquid and solid phases with immersed time (1573 K).

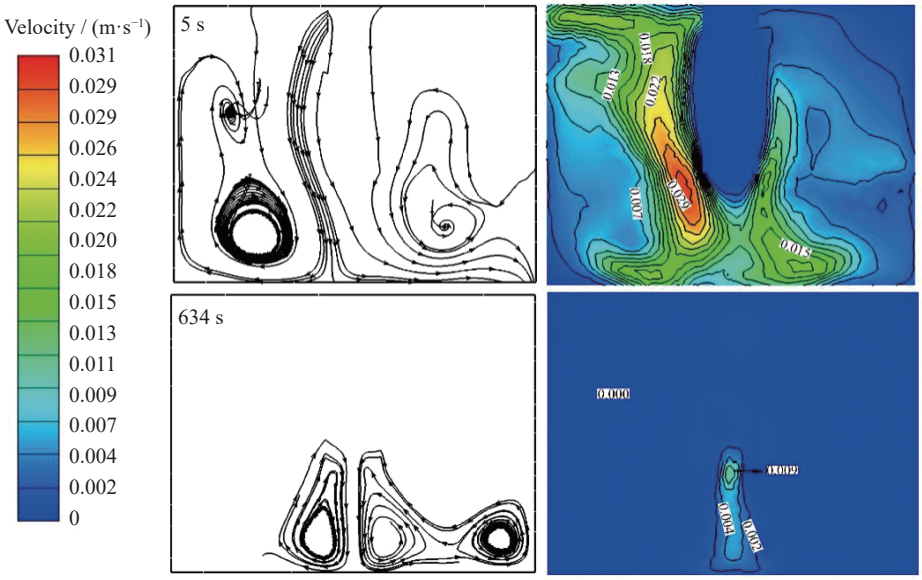

Fig. 7. Changes in the velocity of liquid phase with immersed time (1573 K).

the decrease in density difference until the melting ended. The hot metal flow also slowed down. At 634 s, a temperature difference appeared in a small area (Fig. 8), thereby generating a density difference (Fig. 6). Correspondingly, a weak flow occurred from top to bottom, as shown in Fig. 7. The maximum velocity caused by natural convection was only 0.009 $m \cdot s^{-1}$.

Therefore, the flow of hot metal in a stationary bath conforms to natural convection. The temperature and density difference is large in the early stage of melting, which leads to a violent natural convection. Then, the temperature and density difference gradually decreases and weakens the natural convection until the bath is uniform. Wright also reported that a high-density liquid flows along the vertical solid–liquid interface to form natural convection because of the density difference [26].

The temperature changes are described taking 1573 K as an example in Fig. 8. In the early stage of melting (12 s), the temperature of the scrap cylinder rapidly increased, along with a decrease in bath temperature. At 214 s, the scrap temperature was similar to the bath temperature, except for a small part of the scrap. Chen [20] also reported a similar temperature between the molten pool and the solid scrap after the solidified layer remelted. In addition, the bath temperature was not uniform at the end of the melting (634 s). The minimum temperature was 1563.55 K.

3.3. Carburization during scrap melting

The liquid fraction at the carburization stage is discussed taking 1573 K as an example. As shown in Fig. 9, the liquid fraction gradually increased from 150 to 214 s (dotted box). The top of the scrap cylinder melted at 214 s. Correspondingly, the carbon content increased as shown in Fig. 10. Therefore, the liquid fraction increased with the increase in carbon concentration. The solid scrap melted when the carbon content was high enough to cause its melting point to be lower than the bath temperature. This stage was controlled by the mass transfer of carbon. Chen [20] also indicated that the melting rate of the scrap is determined by the carbon mass transfer when the bath temperature is less than the melting point of scrap. In addition, the phenomenon could be observed in the changes of S/S_0 (Fig. 3). A hump formed, and the melting was not obvious. However, the scrap cylinders melted quickly until the melting ended. As shown in Fig. 11, the time required at the carburization stage decreased from 214 s to 12 s when the bath temperature increased from 1573 K to 1723 K. Therefore, the carburization took obviously longer time at low temperatures than at high temperatures that the effect of carburization on scrap melting could not be ignored at low temperatures.

In addition, the carbon distribution was measured by an electron probe micro-analyzer (EPMA) (SHIMADZU) to prove the existence of carburization. The test samples were a cross-section of the scrap cylinder immersed in hot metal for 5 s and 60 s at 1573 K. A 300 μm ×220 μm area was selected as the measurement domain. In Fig. 12, the sample surface on the right side of the figure is defined as the outer edge of the scrap. The position near the center of the sample is defined as the interior. The carbon content at the surface of scrap was higher than that in the interior, and it gradually decreased from the outer edge to the interior. A sharp interface was found during the changes in carbon content. An explanation could be that the carbon diffused from the high-carbon molten pool to the surface of the low-carbon scrap because of the large concentration gradient. In addition, the carburization depth gradually increased with immersion time. For the

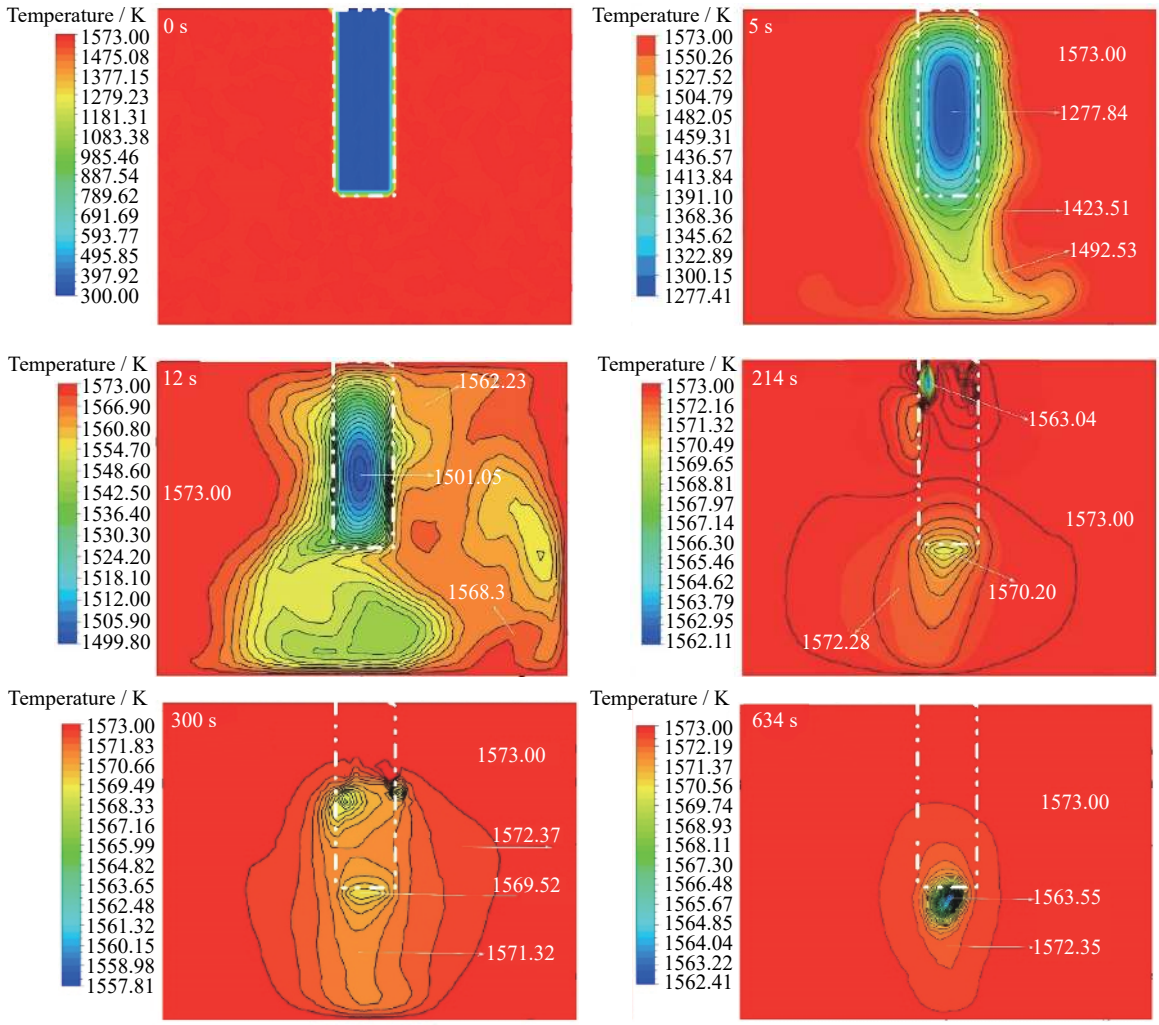

Fig. 8. Changes in the temperature of liquid and solid phases with immersed time (1573 K).

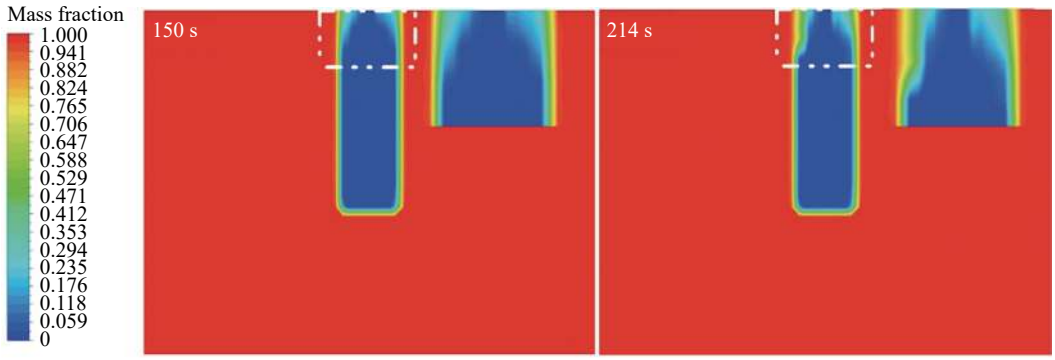

Fig. 9. Changes in the liquid fraction of solid scrap at the carburization stage (1573 K).

sample immersed for 5 s, the thickness of the boundary layer with significant concentration difference was 130 μm. However, it was 140 μm for the sample immersed for 60 s. The increasing rate of the carburization depth was 0.182 $\mu m \cdot s^{-1}$. These results proved the existence of carburization during the scrap melting. Penz *et al*. [15] reported an obvious interface between the parent scrap and the frozen shell by the EPMA-measured carbon distribution. Chen [20] also reported that the melting point of scrap decreases because of the carbon diffusion from the molten pool to its surface. The microstructure of the low-carbon scrap cylinder is affected by the temperature and the carbon content [27–29].

As shown in Fig. 13(a), the phenomenon can be explained by the development of a concentration boundary layer between the hot metal and the surface of the scrap cylinder. In Fig. 13(b), the changes in carbon content are shown in the

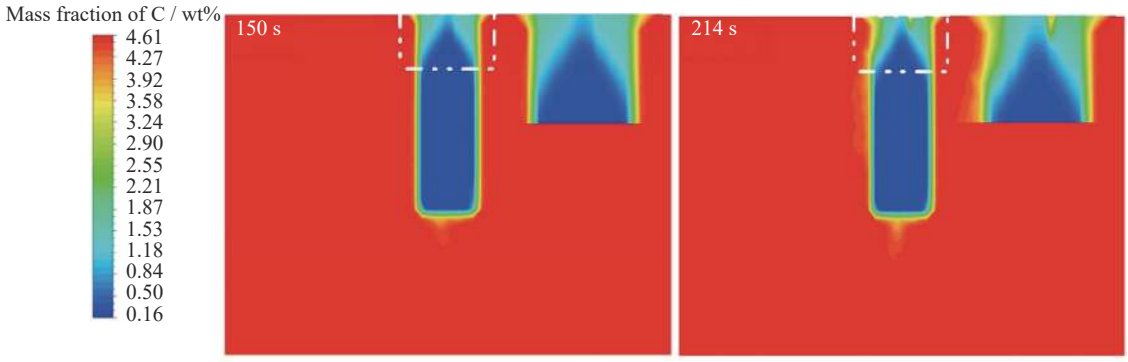

Fig. 10. Changes in carbon concentration of liquid and solid phases at the carburization stage (1573 K).

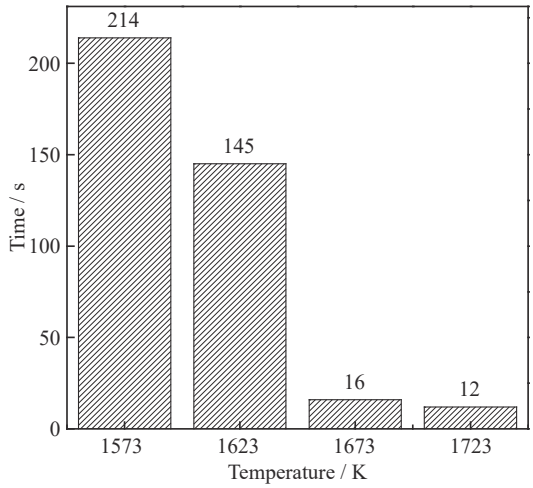

Fig. 11. Time of carburization at different bath temperatures.

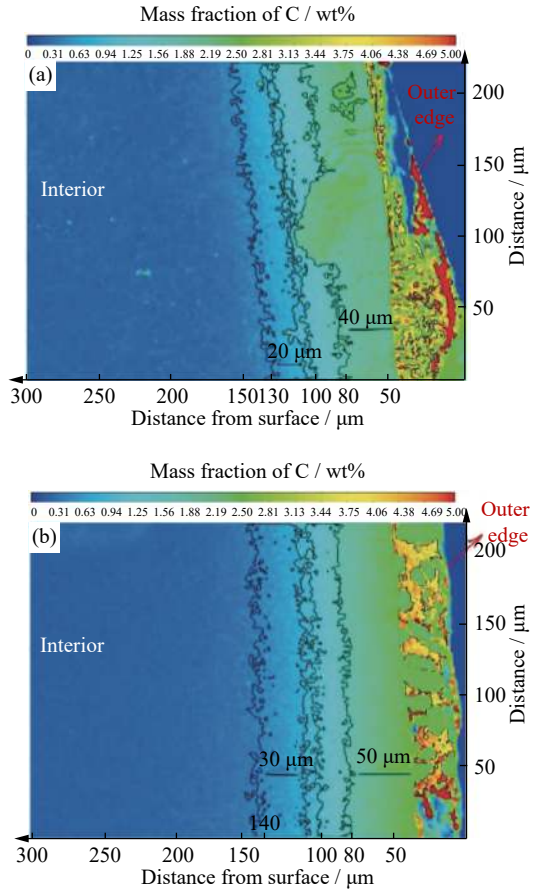

Fig. 12. EPMA-measured carbon distribution at 1573 K: (a) 5 s; (b) 60 s.

Fe-C phase diagram generated by the FactSage (Mn: 0.391wt%, Si: 0.11wt%). In the early stage of melting, the carbon content of the scrap cylinder (C_s) is almost constant until the temperature increases from T_s to $T_{liquidus}$. Where, C_s is the initial carbon content of the scrap in wt%, T_s is the initial temperature of scrap in °C, and $T_{liquidus}$ is the liquidus temperature in °C. Meanwhile, the carbon content increases to $C_{solidus}$ and $C_{liquidus}$. Where, $C_{solidus}$ and $C_{liquidus}$ are the values of the solid and liquid at the interface in wt%, respectively [7,21–24]. The scrap melts when its melting point is less than the bath temperature (T_b). Where, T_b and C_b are the bath temperature in °C and carbon content of hot metal in wt%, respectively. In specific, the carbon concentration gradient promotes the carbon diffusion from the hot metal to the scrap cylinder to decrease the melting point of the scrap cylinder.

4. Conclusions

A numerical simulation was conducted and compared with experimental data to analyze scrap melting under natural convection. The following conclusions were obtained.

(1) A 3D numerical model applying temperature- and carbon concentration-dependent material properties was established to visualize the melting of the scrap cylinders in hot metal, including natural convection and carbon diffusion. The simulated results agreed reasonably well with the experimental ones.

(2) Unlike previous studies, the scrap melting was divided into four stages: formation of a solidified layer, rapid melting of the solidified layer, carburization, and carburization + normal melting. In addition, the bath temperature initially decreased and then increased until the bath temperature was uniform.

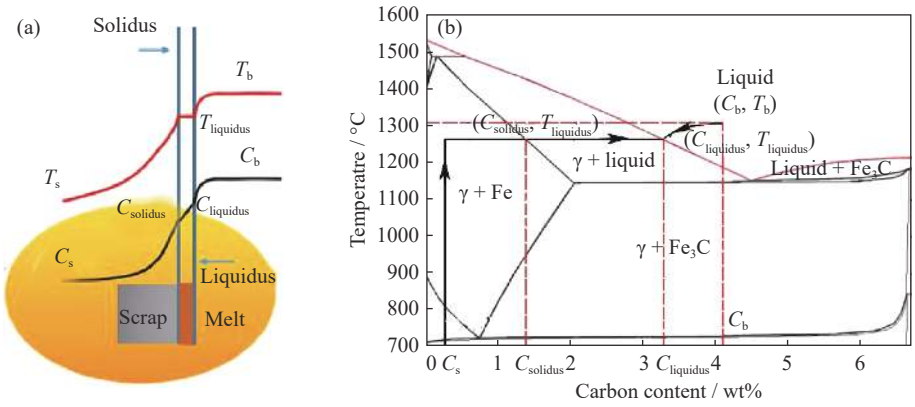

Fig. 13. Scrap melting mechanism: (a) temperature/concentration curve; (b) Fe–Fe_3C phase diagram.

(3) A high-density liquid flowed along the vertical solid–liquid interface to form natural convection from the top to the bottom. The natural convection weakened with the decrease in temperature and density difference. The maximum velocity caused by natural convection reached 0.029 $m \cdot s^{-1}$ at 5 s for the bath temperature of 1573 K. It was only 0.009 $m \cdot s^{-1}$ at the end of melting (634 s).

(4) The phenomenon of carburization was visualized by changes in carbon concentration. The EPMA-measured carbon distribution verified that the carbon content gradually decreased from the outer edge of the parent scrap to the interior. The boundary with significant concentration difference moved from 130 μm to 140 μm when the duration changed from 5 s to 60 s for the bath temperature of 1573 K. In addition, the time required at the carburization stage decreased from 214 s to 12 s when the bath temperature increased from 1573 to 1723 K. The carburization took obviously longer at low temperatures than at high temperatures that the effect of carburization on scrap melting could not be ignored at low temperatures.

Acknowledgements

This work was supported by the National Key R&D Program of China (No. 2019YFC1905701), the National Natural Science Foundation of China (Nos. 51674022 and 51734003), and the Key projects of NSFC (No. U1960201).

References

[1] F. Oeters and R.M. Ni, *Metallurgy of Steelmaking*, The Metallurgical Industry Press, Beijing, 1997, p. 479.
[2] R.D. Pehlke, P.D. Goodell, and R.W. Dunlap, Kinetics of steel dissolution in molten pig iron, *Trans. Metall. Soc. ALME*, 233(1965), p. 1420.
[3] R.I.L. Guthrie and P. Stubbs, Kinetics of scrap melting in baths of molten pig iron, *Can. Metall. Q.*, 12(1973), No. 4, p. 465.
[4] K. Mori and H. Nomura, Study on the rate of scrap melting in the steelmaking process, *Tetsu-to-Hagané*, 55(1969), No. 5, p. 347.
[5] E.M. Gol'dfarb and B.I. Sherstov, Heat and mass transfer when melting scrap in an oxygen converter, *J. Eng. Phys.*, 18(1970), No. 3, p. 342.
[6] D. Weisz-Patrault, Coupled heat conduction and multiphase change problem accounting for thermal contact resistance, *Int. J. Heat Mass Transfer*, 104(2017), p. 595.
[7] A.K. Shukla, B. Deo, and D.G.C. Robertson, Scrap dissolution in molten iron containing carbon for the case of coupled heat and mass transfer control, *Metall. Mater. Trans. B*, 44(2013), No. 6, p. 1407.
[8] Y.K. Wu and M. Lacroix, Numerical simulation of the melting of scrap metal in a circular furnace, *Int. Commun. Heat Mass Transfer*, 22(1995), No. 4, p. 517.
[9] K. Isobe, H. Maede, K. Ozawa, K. Umezawa, and C. Saito, Analysis of the scrap melting rate in high carbon molten iron, *Tetsu-to-Hagané*, 76(1990), No. 11, p. 2033.
[10] A. Kruskopf and S. Louhenkilpi, 1-dimensional scrap melting model for steel converter (BOF), [in] *Proceedings of the MEC & 2nd ESTAD*, Düsseldorf, Germany, 2015, p. 15.
[11] A. Kruskopf, *Multiphysical Modeling Approach for Basic Oxygen Steelmaking Process* [Dissertation], Aalto University, Finland, 2018, p. 12.
[12] A. Kruskopf and V.V. Visuri, A gibbs energy minimization approach for modeling of chemical reactions in a basic oxygen furnace, *Metall. Mater. Trans. B*, 48(2017), No. 6, p. 3281.
[13] S. Deng, A.J. Xu, G. Yang, and H.B. Wang, Analyses and calculation of steel scrap melting in a multifunctional hot metal ladle, *Steel Res. Int.*, 90(2018), No. 3, p. 1.
[14] H.P. Sun, Y.C. Liu, C.C. Lin, and L.U. Muh-Jung, Experimental observation of spherical scrap melting in hot metal, [in] *International Congress on the Science & Technology of Steelmaking*, Beijing, China, 2015, p. 136.
[15] F.M. Penz, J. Schenk, R. Ammer, G. Klösch, K. Pastucha, and M. Reischl, Diffusive steel scrap melting in carbon-saturated hot metal-phenomenological investigation at the solid-liquid interface, *Materials*, 12(2019), No. 8, p. 1358.
[16] M. Gao, S.F. Yang, and Y.L. Zhang, Experimental study on mass transfer during scrap melting in the steelmaking process, *Ironmaking Steelmaking*, (2019), p. 1.
[17] H.L. Zhao, X. Zhao, L.Z. Mu, L.F. Zhang, and L.Q. Yang, Gas-liquid mass transfer and flow phenomena in a peirce-smith converter: a numerical model study, *Int. J. Miner. Metall. Mater.*, 26(2019), No. 9, p. 1092.
[18] J. Dongik, K. Yumkyum, S. Minsoo, and L. Joonho, Kinetics of carbon dissolution of coke in molten iron, *Metall. Mater. Trans. B*, 43(2012), No. 6, p. 1308.

[19] A. Fluent, *ANSYS Fluent Theory Guide, Release 15.0 ed.*, ANSYS Inc., Canonsburg, PA, 2013. ANSYS Inc., USA, 15317, 724.
[20] J.X. Chen, *Metallurgy of Iron and Steel (Steelmaking)*, The Metallurgical Industry Press, Beijing, 2012, p. 174.
[21] J. Szekely, Y.K. Chuang, and J.W. Hlinka, The melting and dissolution of low-carbon steels in iron-carbon melts, *Metall. Mater. Trans. B*, 3(1972), No. 11, p. 2825.
[22] Y.U. Kim and R. Pehlke, Mass transfer during dissolution of a solid into liquid in the iron-carbon system, *Metall. Trans.*, 5(1974), No. 12, p. 2527.
[23] M. Kosaka and S. Minowa, Mass-transfer from solid metal cylinder into liquid metal, *Tetsu-to-Hagane*, 52(1966), No. 12, p. 1748.
[24] M. Kosaka and S. Minowa, Mass-transfer from graphite cylinder into liquid Fe–C alloy, *Tetsu-to- Hagane*, 53(2010), No. 13, p. 1467.
[25] K. Wu, *Principle of Metallurgical Transmission*, Peking University Press, Beijing, 2016, p. 142.
[26] J.K. Wright, Steel dissolution in quiescent and gas stirred Fe/C melts, *Metall. Mater. Trans. B*, 20(1989), No. 3, p. 363.
[27] Z.Y. Liu, Y.P. Bao, M. Wang, X. Li, and F.Z. Zeng, Austenite grain growth of medium carbon alloy steel with aluminum additions during heating process, *Int. J. Miner. Metall. Mater.*, 26(2019), No. 3, p. 282.
[28] V. Dakre, D.R. Peshwe, S.U. Pathak, and A. Likhite, Effect of austenitization temperature on microstructure and mechanical properties of low carbon equivalent carbidic austempered ductile iron, *Int. J. Miner. Metall. Mater.*, 25(2018), No. 7, p. 770.
[29] G.S Wei, R. Zhu, T.P Tang, and K. Dong, Study on the melting characteristics of steel scrap in molten steel, *Ironmaking Steelmaking*, 46(2019), No. 7, p. 609.